New Carbon Materials, 2023, 38(5): 898 -912

Supporting information

A universal strategy for producing 2D functional carbon-rich materials from 2D porous organic polymers for dual-carbon lithium-ion

Xiaoyu Xin[1], Bin Zhao[1], Jinshu Yue[2], Debin Kong[2], Shanke Zhou[3], Xiaoxiong Huang[3], Bin Wang[3], Linjie Zhi[2, 3]*, Zhichang Xiao[1]*

[1]Department of Chemistry, College of Science, Hebei Agricultural University, Baoding 071001, People's Republic of China.

[2]College of New Energy, China University of Petroleum (East China), Qingdao, P. R. China.

[3]CAS Key Laboratory of Nanosystem and Hierarchical Fabrication, National Center for Nanoscience and Technology, Beijing 100190, People's Republic of China.

*Corresponding authors:
E-mail: xiaozhichangcnu@sina.cn (Z. Xiao); zhilj@nanoctr.cn (L. Zhi)

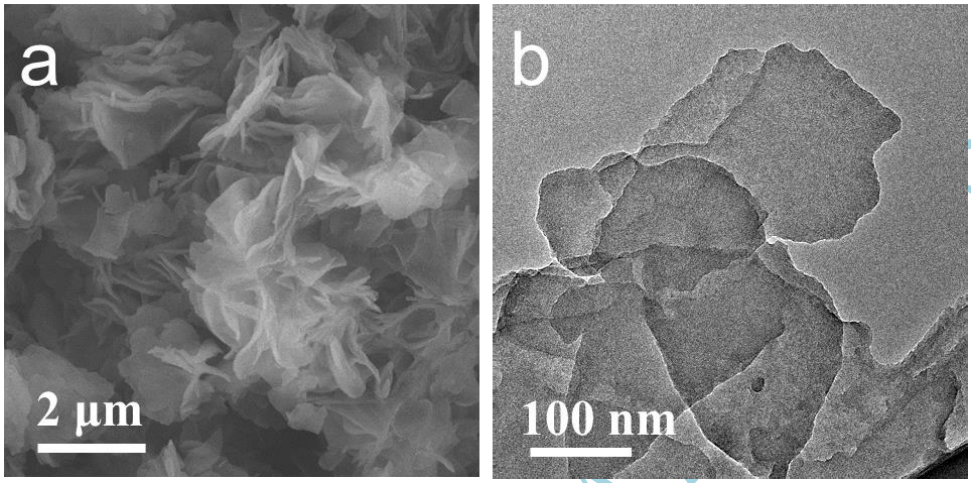

Figure S1. (a) SEM image and (b) TEM image of NPNs.

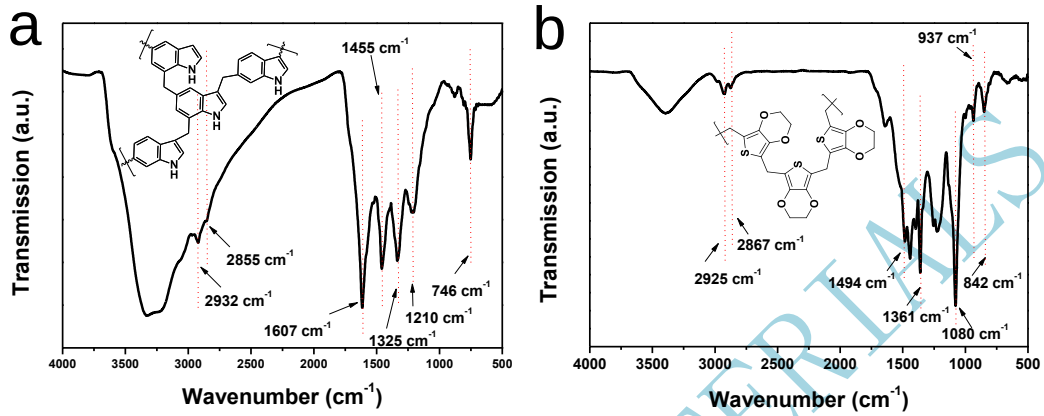

Figure S2. FTIR spectrum of (a) indole-NPNs; (b) EDOT-SPNs.

For indole-NPNs, the peaks at ~1607 and 1455 cm^{-1} represent benzene ring skeleton vibration, while the peaks at ~2932 and 2855 cm^{-1} confirm the existence of methylene. For EDOT-SPNs, the peaks at 1494 and 1361 cm^{-1} were attributed to C–C or C=C stretching of quinoidal structure and ring stretching of thiophene ring, respectively; the peak at 1080 cm^{-1} originated from C–O–C bond stretching in the ethylene dioxy group; peaks at 937 and 842 cm^{-1} corresponds to C–S bond in the thiophene ring while the peaks at ~2925 and 2867 cm^{-1} confirm the existence of methylene.

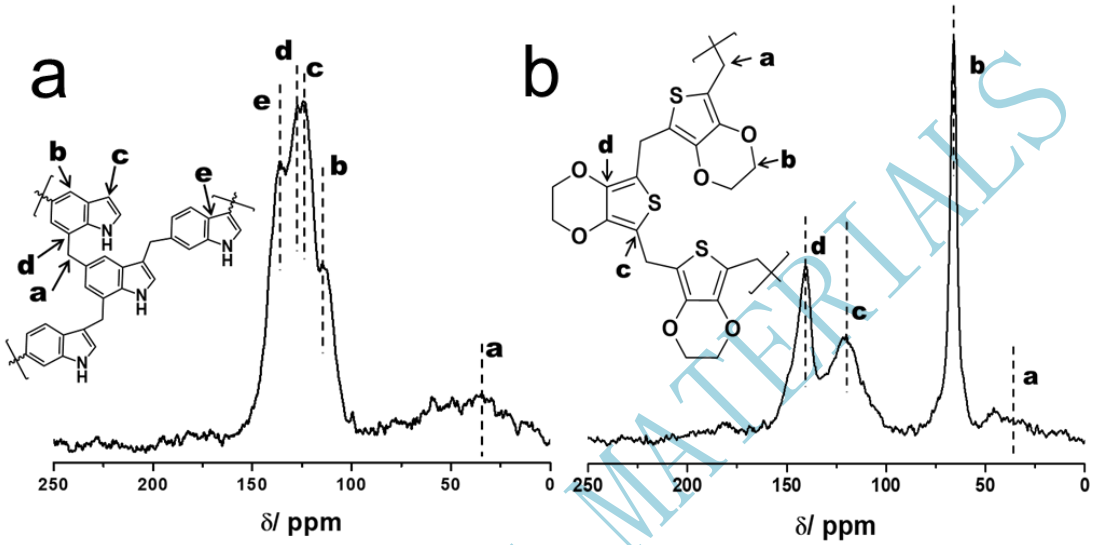

Figure S3. ^{13}C solid state NMR spectrum of (a) indole-NPNs; (b) EDOT-SPNs.

^{13}C SS-NMR spectra of indole-NPNs showed resonance peaks near 135.9 and 127 ppm correspond to substituted aromatic carbon; while the peaks near 124 and 114 ppm correspond to non-substituted aromatic carbon, and the resonance peaks near 31 ppm is assigned to carbon in methylene linker formed after knitting reaction [1].

^{13}C SS-NMR spectra of EDOT-SPNs showed resonance peaks near 140.5 and 120.1 ppm correspond to substituted aromatic carbon and non-substituted aromatic carbon, respectively; and the resonance peaks at 66 and 31 ppm are assigned to methylene linker in and out of the EDOT ring.

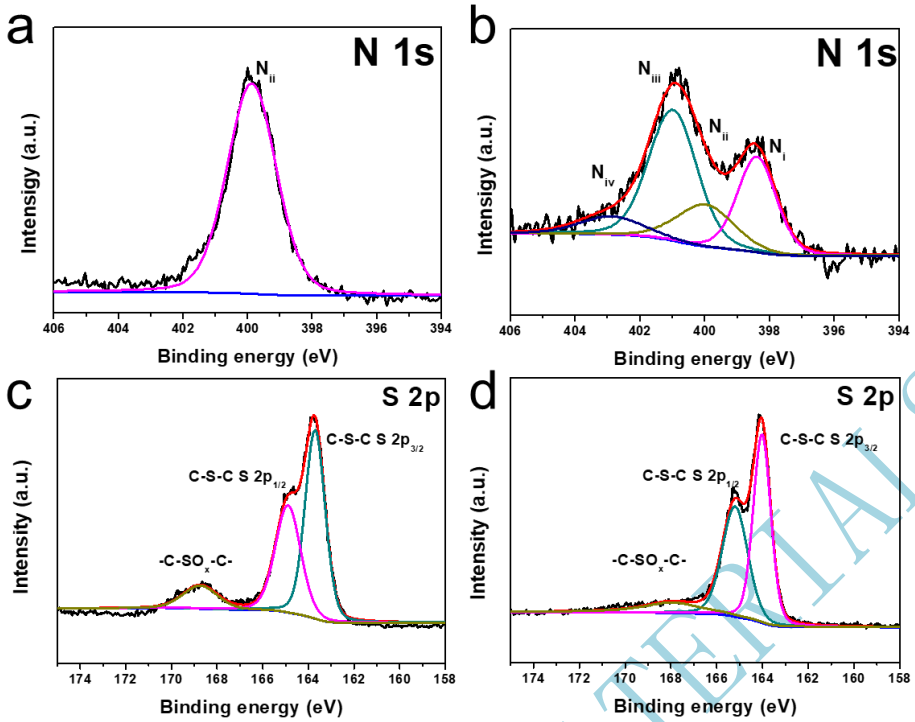

Figure S4. High-resolution XPS spectrum of N1s for (a) indole-NPNs and (b) indole-NCNs; S2p for (c) EDOT-SPNs and (d) EDOT-SCNs.

XPS result further revealed the chemical composition of indole-NPNs. As expected, indole-NPNs displayed only one peak at 399.8 eV, corresponding to N atoms within the pentagonal ring of indole [2], and the nitrogen content is 7.5 at%. Following heat treatment at 800°C, four distinct nitrogen species can be observed, indicating that some N atoms within the pentagonal ring of pyrrole have been converted into other types of nitrogen. This observation is consistent with the behavior seen in pyrrole-based materials. And the nitrogen content of indole-NCNs is still as high as 5.3 at%.

The XPS results reveal the chemical composition of EDOT-SPNs, with a sulfur content of 7.80 at%. As expected, the fine-scanned high-resolution S 2p spectrum of EDOT-SPNs displays the S $2p_{1/2}$ and S $2p_{3/2}$ doublet detected at 164.9 eV and 163.7 eV, with an intensity ratio of about 2:3, corresponding to C-S-C S $2p_{3/2}$ and C-S-C S $2p_{1/2}$, respectively [3, 4]. This result confirms the successful incorporation of EDOT into the polymer. The peak at 168.7 eV is related to -C-SO_x-C- group [5]. Upon high-temperature treatment at 800℃, the S 2p XPS spectrum for EDOT-SCNs is similar in shape to that

of EDOT-SPNs, mainly reflected in the similar relative proportions of C-S-C covalent bonds. However, there are noticeable differences between the two samples. First, the proportion of the C-SO_x-C peak in EDOT-SCNs is significantly reduced after high-temperature treatment, which is probably due to the percentage of C-S-C and C-SO_x-C is temperature-dependent [6]. As the calcination temperature increases, the proportion of C-S-C increases, while the C-SO_x-C group becomes unstable and may decrease or even disappear. Secondly, after high-temperature treatment, the atomic percentage of sulfur decreases to 4.92 at% in EDOT-SCNs. This reduction can be attributed to the atomic rearrangement and condensation reactions of the carbon skeleton during the high-temperature treatment process, which leads to the escape of sulfur atoms from the carbon framework.

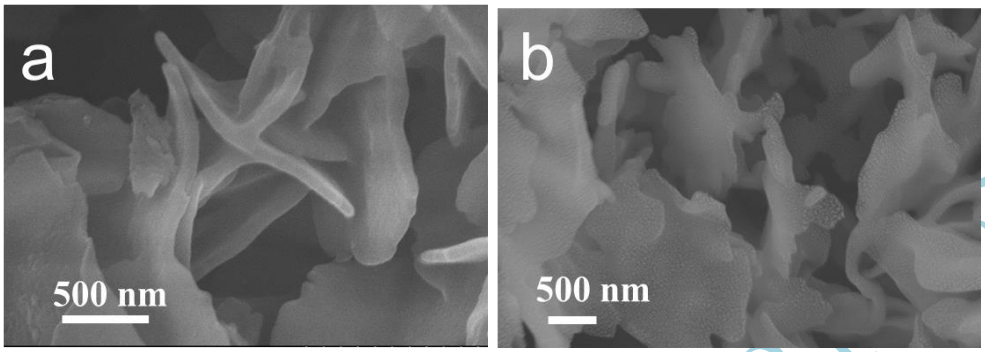

Figure S5. SEM images of (a) indole-NPNs and (b) EDOT-SPNs.

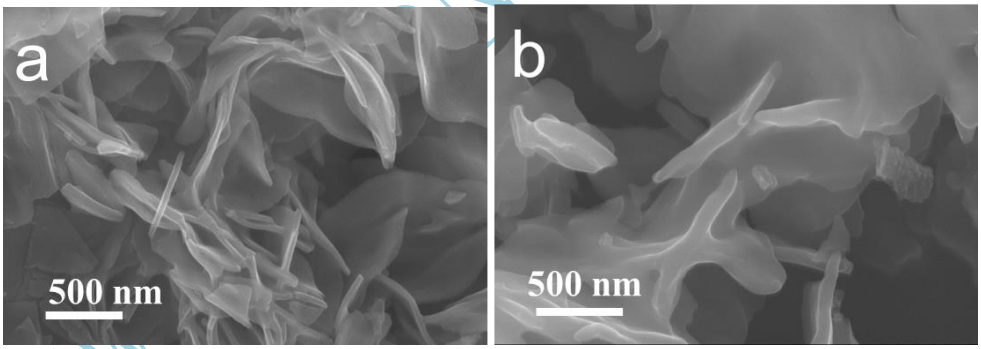

Figure S6. SEM images of (a) indole-NCNs and (b) EDOT-SCNs.

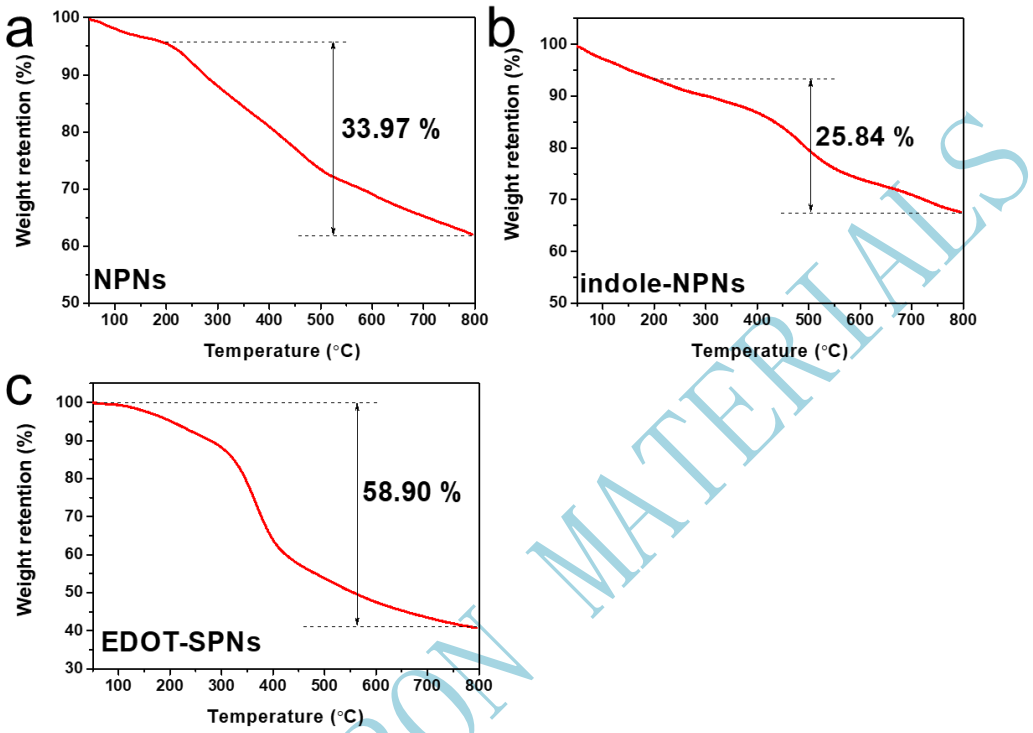

Figure S7. TGA curves of (a) NPNs; (b) indole-NPNs and (c) EDOT-SPNs

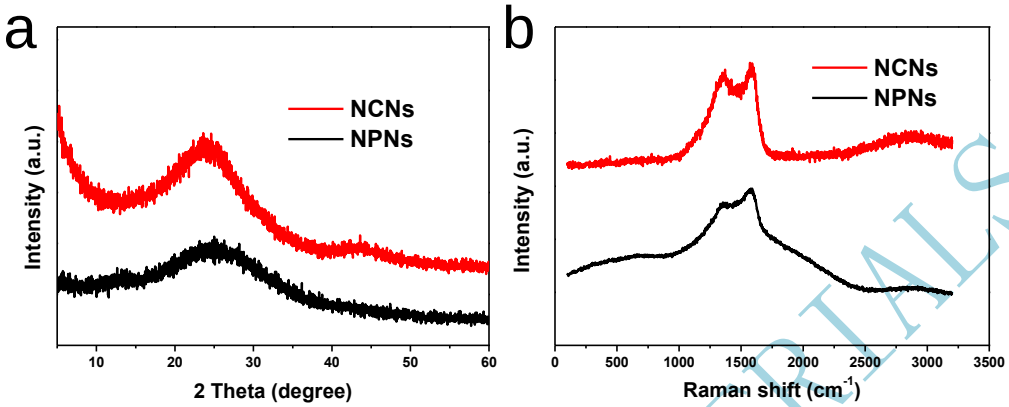

Figure S8. (a) XRD patterns; (b) Raman spectra of NCNs and NPNs

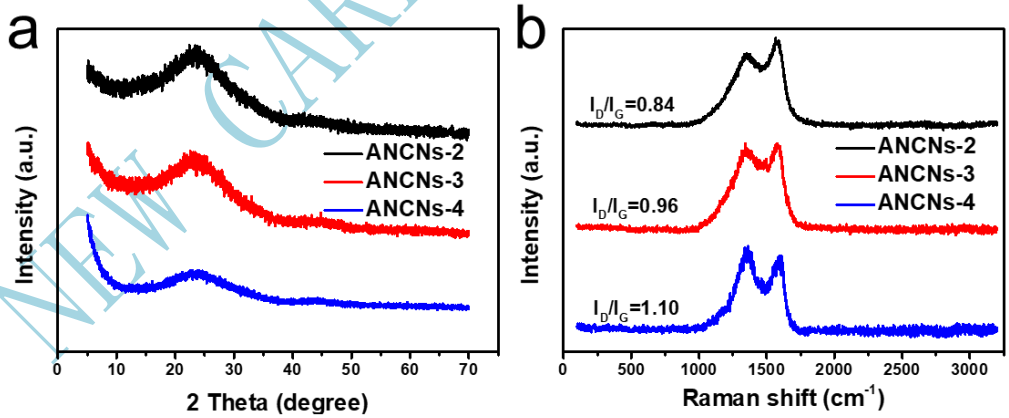

Figure S9. (a) XRD patterns; (b) Raman spectra of ANCNs samples.

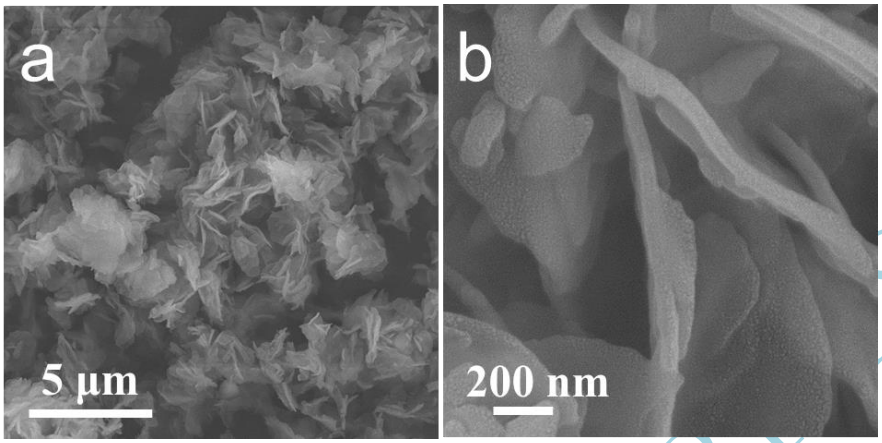

Figure S10. (a)-(b) SEM images of NPNs at different magnification.

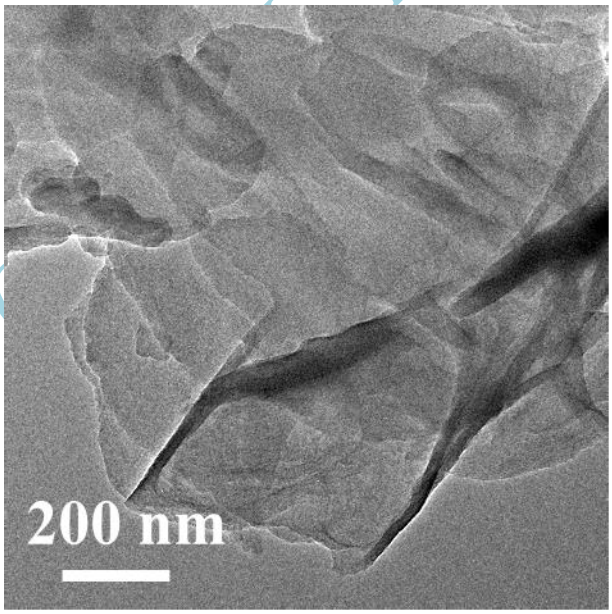

Figure S11. TEM image of NPNs.

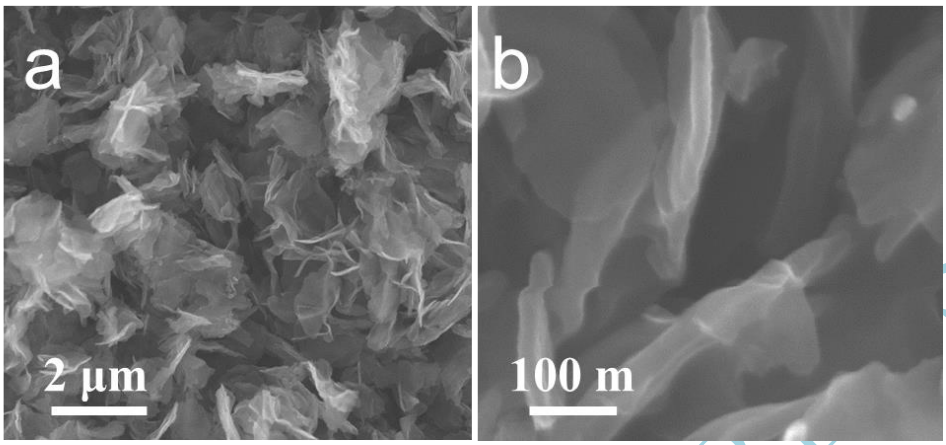

Figure S12. (a)-(b) SEM images of NCNs at different magnification.

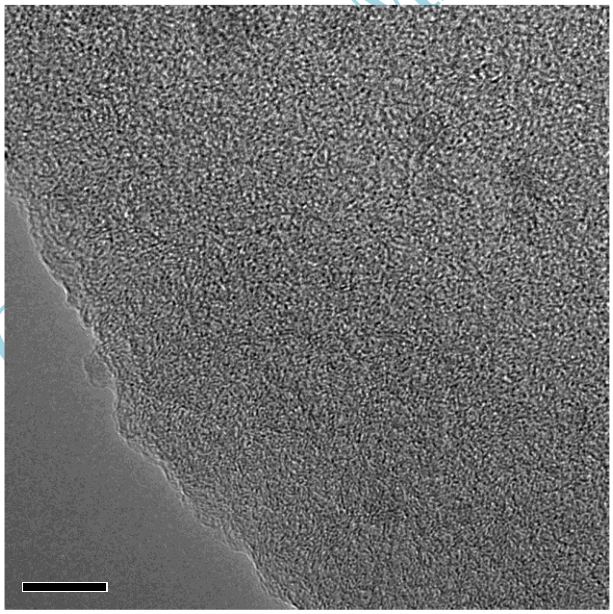

Figure S13. HRTEM image of NCNs.

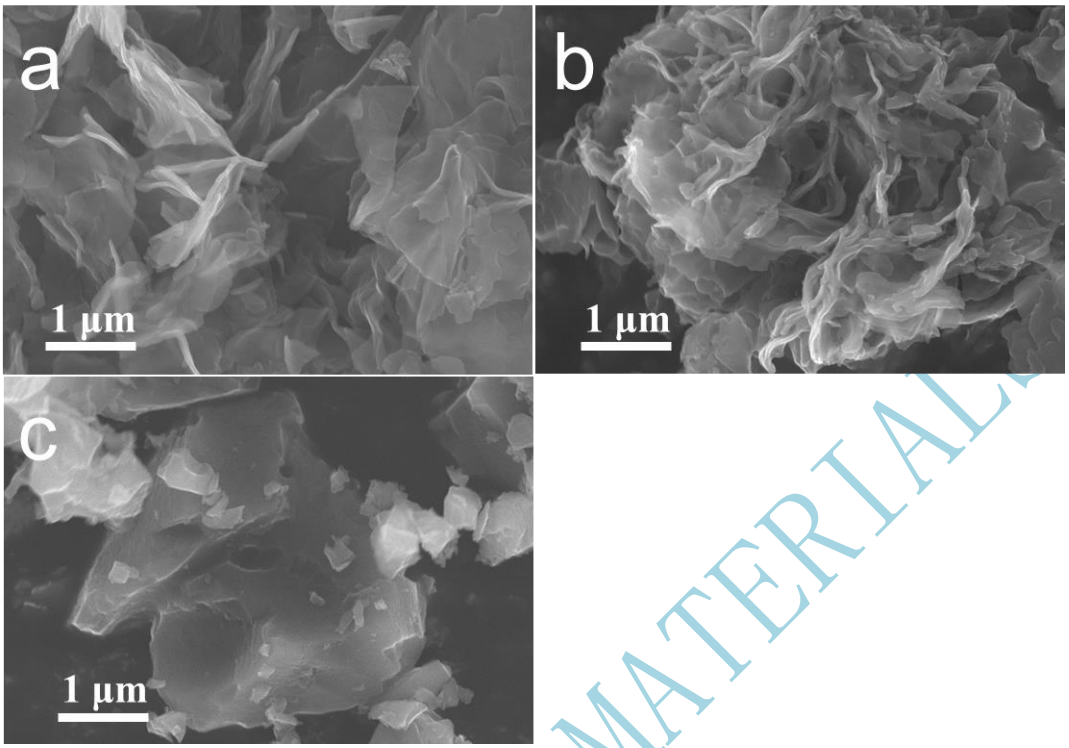

Figure S14. SEM images of (a) ANCNS-2; (b) ANCNS-3; (c) ANCNS-4.

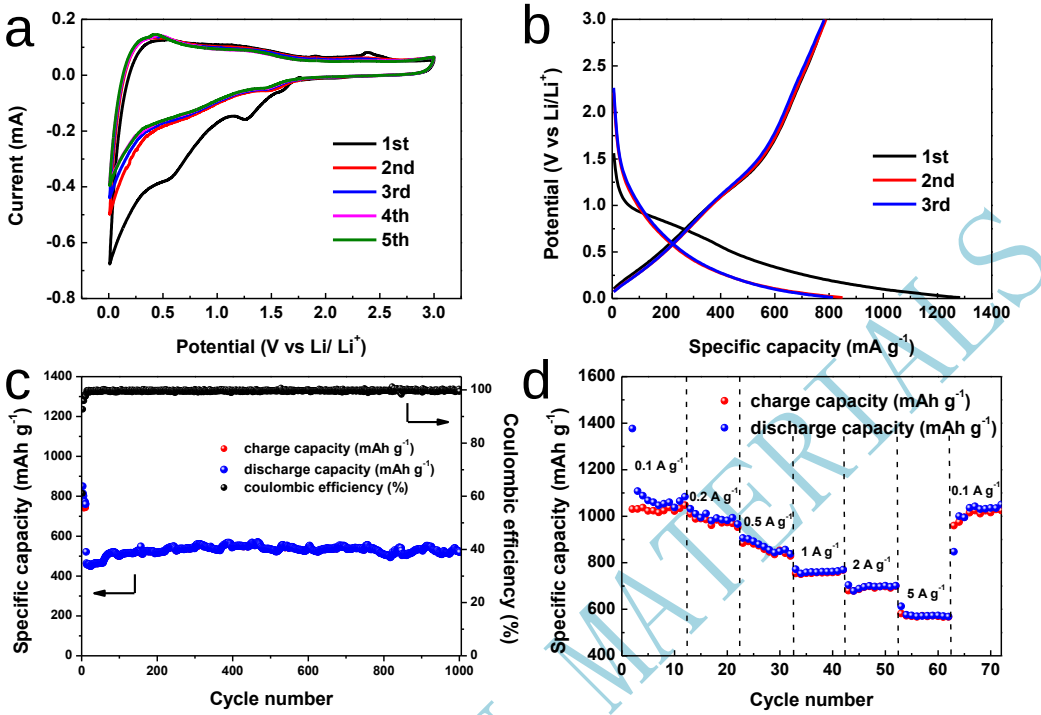

Figure S15. Performance of lithium-ion batteries based on the NCNs: (a) CV curves at a scan rate of 0.2 mV s^{-1}; (b) discharge/ charge voltage profiles; (c) long-term cycling stability at 5 A g^{-1}; (d) rate capability at varied current densities from 0.1 to 5 A g^{-1}.

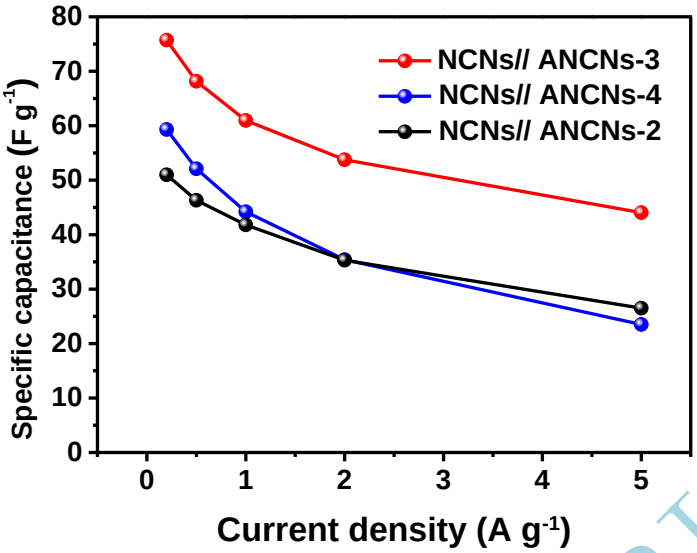

Figure S16. Comparison of the rate capabilities for NCNs// ANCNs LICs.

References

[1] Li B, Gong R, Wang W, et al. A New Strategy to Microporous Polymers: Knitting Rigid Aromatic Building Blocks by External Cross-Linker[J]. Macromolecules, 2011, 44: 2410-2414.

[2] Sun Y, Wang T, Li A, et al. Knitting N-doped Hierarchical Porous Polymers to Stabilize Ultra-small Pd Nanoparticles for Solvent-Free Catalysis[J]. Chemistry-an Asian Journal, 2017, 12: 3039-3045.

[3] Ait El Fakir A, Anfar Z, Enneiymy M, et al. Conjugated polymers templated carbonization to design N, S co-doped finely tunable carbon for enhanced synergistic catalysis[J]. Applied Catalysis B: Environmental, 2022, 300: 120732.

[4] Qin D, Wang L, Zeng X, et al. Tailored edge-heteroatom tri-doping strategy of turbostratic carbon anodes for high-rate performance lithium and sodium-ion batteries[J]. Energy Storage Materials, 2023, 54: 498-507.

[5] Yin B, Liang S, Yu D, et al. Increasing Accessible Subsurface to Improving Rate Capability and Cycling Stability of Sodium-Ion Batteries[J]. Advanced Materials, 2021, e2100808.

[6] Ma G, Ning G, Wei Q. S-doped carbon materials: Synthesis, properties and applications[J]. Carbon, 2022, 195: 328-340.